The Astrophysical Journal, 747:36 (7pp), 2012 March 1 doi:10.1088/0004-637X/747/1/36

METHANE–NITROGEN BINARY NUCLEATION: A NEW MICROPHYSICAL MECHANISM FOR CLOUD FORMATION IN TITAN'S ATMOSPHERE

I-Chun Tsai[1], Mao-Chang Liang[2,3,4], and Jen-Ping Chen[1]
[1] Department of Atmospheric Sciences, National Taiwan University, Taipei 10673, Taiwan; jpchen@as.ntu.edu.tw
[2] Research Center for Environmental Change, Academia Sinica, Taipei, Taiwan
[3] Graduate Institute of Astronomy, National Central University, Jhongli, Taiwan
[4] Institute of Astronomy and Astrophysics, Academia Sinica, Taipei, Taiwan
Received 2011 July 18; accepted 2011 November 30; published 2012 February 13

Abstract

It is known that clouds are present in the troposphere of Titan; however, their formation mechanism, particle size, and chemical composition remain poorly understood. In this study, a two-component (CH_4 and N_2) bin-microphysics model is developed and applied to simulate cloud formation in the troposphere of Titan. A new process, binary nucleation of particles from CH_4 and N_2 gases, is considered. The model is validated and calibrated by recent laboratory experiments that synthesize particle formation in Titan-like environments. Our model simulations show that cloud layers can be formed at about 20 km with a particle size ranging from one to several hundred μm and number concentration 10^{-2} to over 100 cm^{-3} depending on the strength of the vertical updraft. The particles are formed by binary nucleation and grow via the condensation of both CH_4 and N_2 gases, with their N_2 mole fraction varying from $<10\%$ in the nucleation stage to $>30\%$ in the condensation growth stage. The locally occurring CH_4–N_2 binary nucleation mechanism is strong and could potentially be more important than the falling condensation nuclei mechanism assumed in many current models.

Key words: methods: numerical – planets and satellites: atmospheres – planets and satellites: composition

Online-only material: color figure

1. INTRODUCTION

Titan, the largest satellite of Saturn, has a dense atmosphere (1.5 bars) composed of ∼98% nitrogen and ∼2% methane (Kuiper 1944; Trafton 1972). The temperature near the surface is ∼94 K and decreases higher in the troposphere. Various phases (vapor, liquid, and solid) of methane can coexist in the lower part of the troposphere since the thermodynamic condition is close to the triple point of methane (90.67 K). As a result, the "methalogical" cycle, which is similar to the terrestrial hydrological cycle (Atreya et al. 2006) can be produced and maintained.

Evidence of clouds in Titan's atmosphere has clearly been seen, and three types of clouds are categorized: convective methane clouds (Brown et al. 2002; Griffith et al. 1998, 2000, 2005, 2009; Roe et al. 2005; Rodriguez et al. 2009, 2011; Turtle et al. 2009, 2011; Schaller et al. 2006), stratiform ethane clouds (Roe et al. 2002; Griffith et al. 2006; Tokano et al. 2006; Schaller et al. 2006, 2009; Le Mouélic et al. 2012), and high-altitude cirrus containing HCN and HC_3N (Samuelson et al. 2007; Anderson et al. 2010; Anderson & Samuelson 2011). Although the presence of clouds has been established, we do not sufficiently understand their formation mechanisms, particle size distribution, and chemical composition.

There have been many modeling studies of cloud formation in Titan's troposphere focusing on the effects of large-scale circulation (Rannou et al. 2006; Rodriguez et al. 2009) and microphysical processes (Barth & Toon 2003, 2004, 2006). However, the microphysical schemes of these models tend to ignore the nucleation process and start the simulation with a prescribed distribution of cloud condensation nuclei, which are assumed to be either ethane ice precipitating from the lower stratosphere (Samuelson & Mayo 1997), tholin from the middle and upper atmospheres (Rannou et al. 2004, 2006), or a combination of both (Barth and Toon 2003, 2004, 2006; Barth & Rafkin 2007). No relevant laboratory validation was done until Wang et al. (2010), who reported the formation of methane/nitrogen droplets in an aerosol chamber under a condition similar to that of Titan. This laboratory experiment provides a unique constraint for convective methane/nitrogen cloud formation in the troposphere.

This study attempts to understand cloud formation on Titan using a multi-component microphysical model, which is validated by the laboratory result of Wang et al. (2010). Then we apply the model to simulate Titan's methane cloud formation. Uncertainties of the model and implications for microphysical processes such as CH_4–N_2 binary nucleation occurring on Titan are presented and discussed.

2. MULTI-COMPONENT MICROPHYSICAL MODEL

The multi-component microphysical model used for the study is modified from the previous model (Chen & Lamb 1994) originally designed for studying liquid- and ice-phase cloud microphysical processes and aerosol formation on Earth (Chen et al. 1997, 2011; Chen & Lamb 1999). The multi-component model considers the thermodynamic and kinetic properties of several chemical species simultaneously involved in their microphysical processes so that the changes in particle chemical compositions and phases can be calculated accordingly. We modify the model for the CH_4–N_2 system of Titan, using 100 mass bins (or classes) for each of the CH_4 and N_2 components. A bin-sizing factor of $\sqrt{2}$ is applied to successively smaller bin limits. Variables tracked for each bin include the particle number concentration and mean mass of each chemical component. The mean mass is allowed to vary within the bin limits so that the sub-bin number distribution can be derived for more accurate computation of mass growth using a method-of-moments type numerical scheme (see Chen & Lamb 1994).

Table 1
Physical–Chemical Parameters Used in the Model

Parameter	Methane	Nitrogen	References
Saturation pressure (kPa)	$10^{\frac{(8.28-0.165\,T)}{(1-0.028\,T)}}$	$10^{\left[5.9379365-\frac{304.48221}{T}\right]}$	Kirk & Ziegler 1965; Lide 1992
Liquid density (kg m^{-3})	415.0	808.0	Wagner 1973
Surface tension (mN m^{-1})	$43.056\cdot\left(1-\frac{T}{199.3}\right)^{1.5}$	$35.464\cdot\left(1-\frac{T}{130.5}\right)^{1.5}$	Blagoi 1960; Fuks & Bellemans 1966; Upstill & Evans 1977
Latent heat (J kg^{-1})	$675443.7-1439.584\cdot T$	$231347.16-0.0699\cdot T^3$	Thompson et al. 1992
Chemical activity [a]	$\exp\{x_{N_2}^2[(a-3b+5c)+4(b-4c)x_{N_2}+12cx_{N_2}^2]\}$	$\exp\{x_{CH_4}^2[a-b(1-4x_{N_2})+c(1-8x_{N_2}+12x_{N_2}^2)]\}$	Thompson et al. 1992

Notes. [a] $a=0.8096-\frac{52.07}{T}+\frac{5443}{T^2}$, $b=-0.0829+\frac{9.34}{T}$, $c=0.072-\frac{6.27}{T}$.

Microphysical processes considered here include nucleation, Brownian coagulation, and condensation. We use the classical stochastic nucleation theory for the binary nucleation (see, for example, Doyle 1961; Seinfeld & Pandis 2006, pp. 514–520). The Brownian collision is calculated according to Fuchs (1964). The condensation growth follows the two-stream Maxwellian theory with consideration of the curvature and solute effects on the particle surface vapor pressure as well as the surface-gas-kinetic effect (see Pruppacher & Klett 1997). As the microphysical model will run in the parcel mode, which is of a zero-dimensional nature, particle sedimentation (fallout) is neglected. The gravitation-induced interaction between particles is also ignored because no measurement of the collision–coalescence efficiencies is available for CH_4–N_2 particles.

Under high-altitude temperature conditions, the methane–nitrogen droplets may freeze into solid particles. This may result in more CH_4 deposition because of the lower saturation vapor pressure in the ice phase. At the same time, N_2 condensation (dissolution) that occurs in the liquid phase may be largely suppressed. Coagulation between particles can also be very different after freezing. The initiation of droplet freezing (i.e., homogeneous nucleation) as well as the subsequent processes mentioned above is considerably more complicated than in the liquid phase and is thus ignored in this study. This omission might not greatly influence our conclusion because the key parameter for both liquid and solid microphysical processes is the particle number concentration, which is determined by the binary nucleation process in this study. The clouds on Earth may serve as an analogy because the ice-phase processes are important but not necessary for cloud and precipitation formation (cf. Lamb & Verlinde 2011, Chap. 12).

Summarized in Table 1 are the physical–chemical parameters needed for describing the CH_4–N_2 system: the surface tension and density of liquid droplets, as well as the saturation vapor pressure, latent heat, chemical activities, and accommodation coefficients of individual component. The liquid density and accommodation coefficient for pure CH_4 and N_2 are assumed to be constant. Other parameters having strong temperature dependence are fitted using the mathematical formulae given in Table 1. The saturation vapor pressure follows the Antoine equation. The latent heat of condensation is fitted by a linear function and the surface tension is fitted following the van der Waals rule. The correlation for the above fittings has an R^2 coefficient >0.999. The surface tension σ and density ρ for the CH_4–N_2 mixture are calculated using the mixture law (see Chen 1994):

$$\sigma=\sum_i x_i\sigma_i \quad (1)$$

$$\rho=\frac{\sum_i x_i M_i}{\sum_i x_i v_i}, \quad (2)$$

where the subscript $i=1, 2$ indicates the chemical species (CH_4 and N_2 in this work), x the mole fraction, M the molecular weight, and v the specific volume. The activity coefficients of CH_4 and N_2 in the solution are calculated based on Thompson et al. (1992). The accommodation coefficient needed for calculating the gas-kinetic effect on the condensation growth for small droplets is not available. We prescribe a value and present the sensitivity of the model results to the changes of this parameter in Section 3.2.

3. LABORATORY SIMULATION

3.1. Model Validation

Using a low-temperature aerosol cell of Firanescu et al. (2006), Wang et al. (2010) carried out experiments at conditions similar to Titan's troposphere at about 13–19 km (temperature of 78–82 K, pressure of 540–760 hPa, and methane mixing ratio of 0.02–0.03). The cell was initially filled with N_2 and CH_4 gases at the above proportion. A baseline experiment was done by injecting pure N_2 into the cell, which did not produce a cloud. When the injected plume was replaced with CH_4, cloud formation was readily visible. The authors concluded that super-cooled CH_4 droplets containing $\sim 30\% \pm 7\%$ of N_2 can be formed at the low to mid-level cloud conditions on Titan. The obtained N_2 mole fraction can be explained by a Monte Carlo simulation for which the vapor–liquid equilibration is assumed (Firanescu et al. 2011). The N_2 mole fraction obtained by the Monte Carlo method can readily be reproduced by the kinetic approach discussed below.

We developed a multi-component microphysics model to simulate processes involved in the aforementioned laboratory experiments to advance our knowledge of microphysics. Figure 1 shows a schematic diagram of the approach to simulate the particle formation made by the above laboratory work. We first consider a pure N_2 injection (the baseline experiment) to the chamber at an initial temperature 78.5 K and pressure 551 hPa (which corresponds to 17.5 km on Titan). This baseline experiment is used to constrain the thermal history of the gas plume in the cell: the injection causes compression warming in the cell followed by subsequent cooling by air mixing and conduction to the wall. The mixing process typically takes the form of exponential decay in temperature. Yet, the characteristic time constant of mixing between the plume and surrounding air and that of conduction to the wall in Wang et al. (2010) are not available to us. Using the baseline experiment, we constrain the mixing time constant to be 4 s and conduction time to be 100 s (see Figure 2). In the chamber experiment (Wang et al. 2010), the gas is injected from a steel cylinder in which the pressure is 3 bars and the temperature is at room temperature. The plume

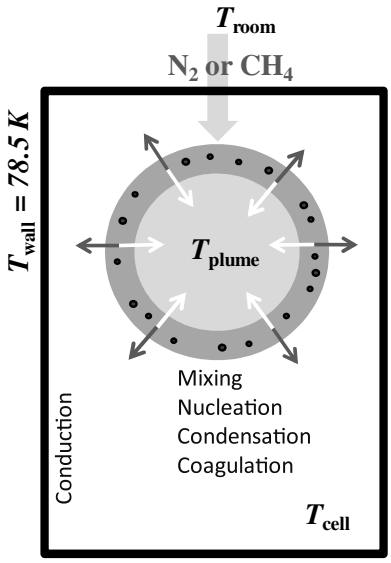

Figure 1. Schematic diagram of model setup. The cell is pre-filled with N_2 and CH_4 gases and the wall temperature is fixed at 78.5 K. The gray shaded circle represents the gas plume. The processes considered are nucleation, condensation, coagulation, conduction cooling, and gaseous mixing.

cools down during injection primarily due to expansion and also conduction to the wall of the injection nozzle. The temperature due to cooling by adiabatic expansion alone is estimated to be 185 K. At this temperature, the pressure in the aerosol cell would reach 650 hPa, higher than the 587 hPa initial pressure measured (Wang et al. 2010). The measured pressure constrains the initial temperature of the injected plume to be as low as 97 K. We attribute the difference to the conduction cooling in the injection nozzle. The same cooling time constants and thermal history are applied to the CH_4 injection experiment. The mixing of the injected warmer CH_4 plume with the cold surrounding air increases the supersaturation of CH_4, the key factor for initiating droplet formation.

In the N_2 plume experiment, the total pressure was raised by 37 hPa immediately after the injection. It then decreased due to cooling and eventually reached a steady value with an excess half of the initial pressure rise. With the CH_4 injection, the total pressure after 20 s becomes lower than the pressure before the plume injection. This reduction is due to particle formation, which is initiated by CH_4–N_2 binary nucleation instead of CH_4 monomolecular nucleation. Although the CH_4 vapor is supersaturated after injecting the plume to the system, the degree of supersaturation is too low to initiate monomolecular nucleation which requires saturation ratios well above 25. The presence of N_2 gas allows binary nucleation, which significantly lowers the required saturation of methane to ~3. Subsequent condensation grows the particle size to ~one to tens of μm, depending on the degree of coagulation. Without considering coagulation, the particle number concentration reaches 10^{11} cm^{-3} and the mean radius after 20 s of simulation is about 1.5 μm. If the coagulation due to Brownian motion is imposed, the number concentration decreases significantly to 10^7 cm^{-3} with the mean radius increased to 20 μm. The mean particle radius estimated from the laboratory results is about several μm, which falls in between the values obtained from simulations with and without the Brownian coagulation process. Such uncertainty is rather small considering the unknowns in the theories of binary nucleation and Brownian coagulation. During particle formation, N_2 can also condense onto the droplets mainly because of its moderate solubility in liquid CH_4. The simulated mole fraction of dissolved N_2 was about 30%, in excellent agreement with the reported laboratory value of 30% ± 7% (Wang et al. 2010). Another simulation was done at a lower temperature and pressure (78 K and 535 hPa; the condition at 19 km from the surface of Titan). The resulting particle density is higher (~10^{14} cm^{-3}) but the size is smaller (1–5 μm; not shown here), which is also consistent with the laboratory results.

3.2. Sensitivity Tests

The calculations presented above contain several major uncertainties. In most microphysical models, surface tension is

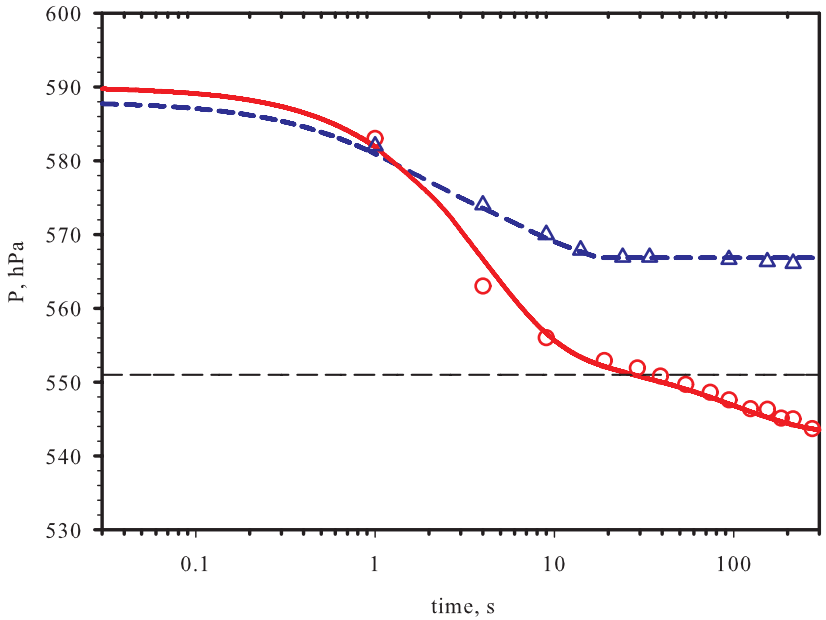

Figure 2. Time evolutions of cell pressure. The symbols (triangle: N2 plume; circle: CH_4 plume) are the laboratory results of Wang et al. (2010); and the curves (solid: N_2 plume; dotted: CH_4 plume) are the simulation results. The horizontal dashed line indicates the initial pressure (551 hPa).
(A color version of this figure is available in the online journal.)

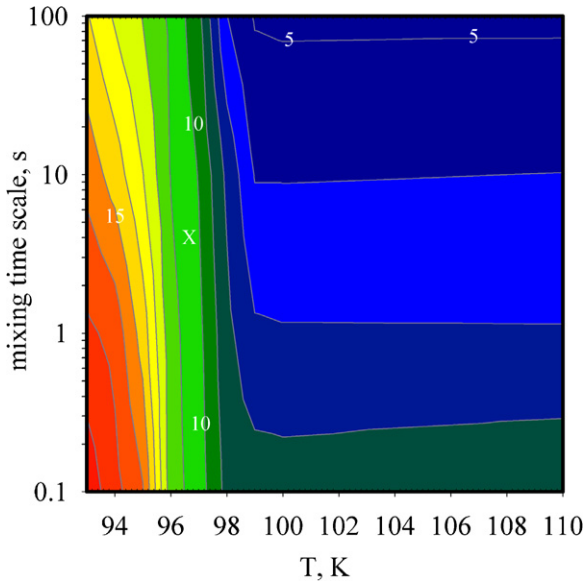

Figure 3. Maximum particle number concentration under different mixing timescales (vertical axis) and initial temperatures (horizontal axis). The contours are number concentration in base-10 logarithmic scale (i.e., "10" indicates 10^{10} cm^{-3}). The "X" marks the values used in this work.

usually assumed to be independent of particle size. However, it actually gets weaker as the particle becomes smaller (Dufour & Defay 1963), particularly for the nucleation germ sizes. This weakening in surface tension can lead to significantly stronger nucleation (Chen et al. 2011). Thus, our model considers the size effect on surface tension based on Chen et al. (2008). Without considering this effect, the particle number concentration would reduce significantly from 10^{11} to 10^{6} cm^{-3}, which is far too low to explain the experimental results.

Another uncertainty is the value of the accommodation coefficient α (also called sticking coefficient or condensation coefficient) which represents the fraction of impinging molecules that do stick to the surface of particles (Fuchs 1959); its value falls between 0 and 1. At the higher end of this range, the condensation process is diffusion limited. At the lower end, it is gas-kinetic limited and is particularly important when the particle is small. For the gas-kinetic limited situation, smaller α results in a slower condensation of vapor, which, in turn, leads to a higher supersaturation and stronger nucleation. For N_2 and CH_4 gases, α ranges from ~0.8 to 1 at room temperature (Bentz et al. 1997). The values at low temperatures are not available but are generally higher than 0.8 (see, for example, Wanlass & Eyring 1961; Trilling 1971) and could be as high as unity at Titan's temperatures. Sensitivity tests show that by varying α from 0.01 to 1.0 the resulting particle number density changes by <20% only. The main reason for this insensitivity is that the nucleation and condensation processes are self-limited: more particles lead to stronger condensation which suppresses nucleation.

Uncertainties also exist in parameters related to the experiments, including the mixing timescale between the injected gas and ambient gas and initial temperature of the injected gas. Sensitivity of the particle number concentration to the mixing time and initial temperature is shown in Figure 3. The Brownian collision is turned off for this test, so that steady-state solutions can be reached. One can see that the particle number concentration is more sensitive to the initial plume temperature for temperatures below 98 K and to the mixing time at higher temperatures. This sensitivity demonstrates that binary nucleation is strongly dependent on the saturation ratios (or temperature) of CH_4 and N_2. Significant nucleation occurs only when the initial plume temperature is less than 98 K. Above 98 K, nucleation is too slow to produce the number of particles measured by Wang et al. (2010), even if the plume can be cooled down faster by mixing. Therefore, the initial plume temperature is critical for our calculation. Note that the initial plume temperature of 97 K that we estimate from the measured initial pressure is only one degree within the margin of significant nucleation. Future laboratory experiments are urgently needed to provide direct measurement to verify our estimation of the dependence of number density with the initial plume temperature and mixing properties. Cooling due to mixing is of secondary importance, as indicated by the gradual change of particle number with mixing time shown in Figure 3. But mixing is essential, as it provides N_2 to initiate binary nucleation.

4. APPLICATION TO TITAN

Convection could play an important role in Titan's methane cycle (Brown et al. 2002; Griffith et al. 2005, 2009; Roe et al. 2005; Schaller et al. 2006). Vertical lifting causes expansion cooling, resulting in an increase in saturation ratio critical for particle nucleation and condensation growth. Using the Huygens probe data, Bird et al. (2005) show that the zonal wind in the lower troposphere is weak (about 1 m s^{-1}) and the vertical wind is even weaker. However, some observation and simulation studies indicate that updrafts near the cloud layer may reach 10 m s^{-1} (Griffith et al. 2005; Hueso & Sánchez-Lavega 2006; Barth & Rafkin 2007), at least locally. Therefore, we run the microphysical model in the adiabatic parcel mode to simulate cloud formation at a range of updraft speeds. The parcel is released at 10 km in height where CH_4 is suggested to be saturated (Atreya et al. 2006). The pressure, temperature, and CH_4 mixing ratio at this level are set at 870 hPa, 83.6 K, and 0.049, respectively.

Figure 4 shows the simulated vertical profiles of the nucleation rate (J), saturation ratio of methane (S_{CH_4}), number concentration (N), mean particle radius (r), optical thickness (τ), and N_2 mole fraction at updraft speeds of 0.01, 0.1, 1.0, and 10.0 m s^{-1}. Because of adiabatic cooling, which elevates the saturation ratios of CH_4 and N_2, the nucleation rate increases exponentially with height and reaches a peak value of about 10^{-3} to 10^{4} m^{-3} s^{-1} at 19–20 km, depending on the updraft speed. The nucleation is then greatly reduced due to depletion of gaseous CH_4 and N_2 by the nucleated particles. Figure 4(a) demonstrates that temperature (or saturation ratios to be exact) is the primary factor for controlling the binary nucleation, as the curves follow each other closely in the early stage of nucleation. This feature was also seen in Figure 3. The nucleation rate becomes significant when the CH_4 saturation ratio reaches about 400% (Figure 4(b)), and its maximum value is proportional to the vertical velocity. Subsequent condensation greatly depletes CH_4 vapor, and therefore further nucleation is prohibited. Thus, strong nucleation occurs within a narrow layer, and its peak may be used to define the cloud base which is at about 19–20 km under the specified condition. Without the participation of N_2, nucleation by CH_4 alone is insignificant (see the dashed curve of Figure 4(a)). Note that currently there is no report of such high CH_4 saturation ratio. For example, the high-resolution Huygens probe data show that atmospheric CH_4 becomes saturated at about 8 km and remains roughly so up to 20 km (Niemann et al. 2005; Atreya et al. 2006). However, our simulations do

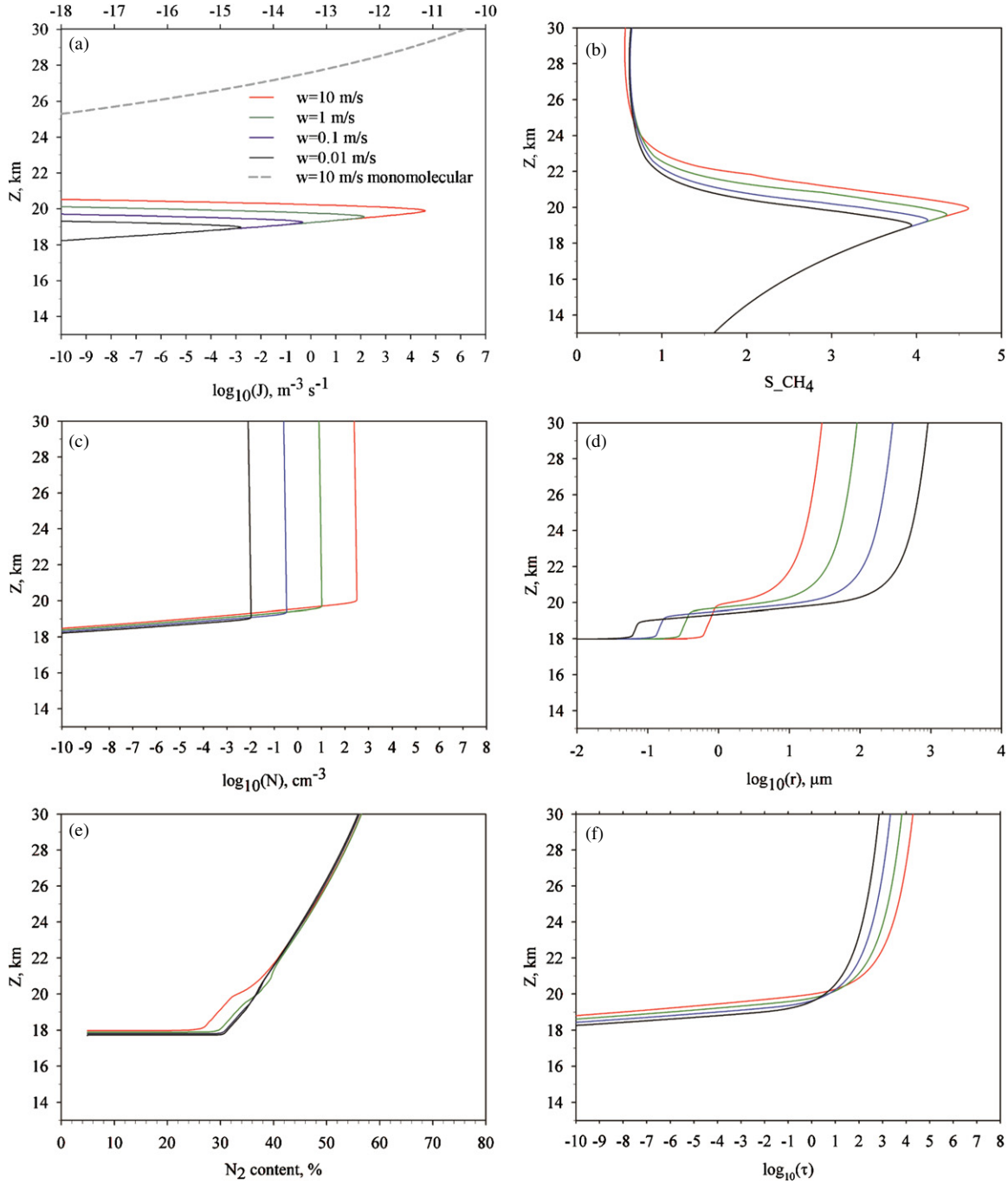

Figure 4. Vertical profiles of convective cloud properties simulated with an adiabatic parcel model-lifted from 10 to 30 km: (a) nucleation rate (m^{-3} s^{-1}, in $\log_{10}$ scale), (b) saturation ratio of methane, (c) number concentration (cm^{-3}, in $\log_{10}$ scale), (d) mean particle radius (μm, in $\log_{10}$ scale), (e) mean N_2 mole fraction in the particles, and (f) cloud optical thickness (in $\log_{10}$ scale) integrated from the cloud base. The thin solid curves are for binary nucleation under various updraft speeds (red line: 10 m s^{-1}, green line: 1 m s^{-1}, blue line: 0.1 m s^{-1}, black line: 0.01 m s^{-1}) with scales shown in the bottom axis. The dashed curve in panel (a) shows rates of monomolecular homogeneous nucleation of CH_4 at the 10 m s^{-1} updraft speed with scales shown in the top axis.

not necessarily contradict with the observations, as the elevated supersaturation of CH_4 (400%) requires the presence of convections which is generally rather localized. It is likely that the Huygens probe missed the convective zones.

Updraft speed (or the cooling rate) is of secondary importance to particle nucleation; it regulates the maximum number of particles that can be formed (Figure 4(c)). For stronger updrafts, the number concentration is lower below the cloud base. The reason for this is that there is less time for nucleation. Above the cloud base, the particle number concentration increases significantly with altitude. Such strong dependence is due to stronger cooling and supply of saturated CH_4, as well as less time for condensation, so that nucleation is enhanced accordingly. Changing the updraft speed by a factor of 10 changes the final particle concentration by a factor of about 30. The Brownian collision process is not significant under the conditions we consider here because the particles are too big to have significant Brownian motion. Including the Brownian coagulation would reduce the concentration by about 5% only. However, for particles of such sizes, gravitational collision–coalescence should cause a significant reduction in particle number, resulting in the formation of precipitable

particles. This coalescence and subsequent fallout processes cannot be simulated realistically by the parcel model. In this regard, the value of number concentration (and thus optical depth) shown in Figure 4(c) should represent an upper limit. For convective clouds on Earth, the reduction of cloud droplets due to precipitation processes is typically within a factor of 10, which can be taken as potential error from ignoring gravitational collision.

The dependence of cloud particle concentration on updraft speed is very similar to the cloud formation on Earth, where cooling in updraft provides a source of condensable vapor (i.e., supersaturation) which is balanced by the depletion of vapor due to condensation. Hence, a stronger updraft gives a stronger source of condensable vapor and thus causes a higher supersaturation which, in turn, allows stronger nucleation. The effect is also similar to the mixing-induced cooling effect in the cell experiment (see Figure 3). The number concentration reaches a peak value just above the cloud base and then decreases slightly due to Brownian collision coalescence as well as parcel expansion.

At an updraft speed of 10 m s^{-1}, the simulated mean particle radius varies from about 1 μm near the cloud base up to 700 μm aloft (Figure 4(d)). The change of particle size with updraft speed is strongly related to the change in number concentration shown in Figure 4(c). For weaker updrafts, the mean radii are smaller at the cloud base but larger as the parcel gets higher. There are two regimes of particle evolution (Figure 4(d)): one near the cloud base and the other above the cloud base. In the first regime, the newly nucleated particles first grow quickly and then slow down as more particles emerge and compete for vapors. The second regime starts when the particle number concentrations reach their maxima, and hence, the growth of particle is determined by further cooling and the available vapor for condensation. This regime shift is also related to the evolution of chemical composition shown in Figure 4(e). The N_2 fraction in the newly formed particle (i.e., the critical embryo) determined by the nucleation theory is around 10%, but the fraction determined by condensation (dissolution) is about 30% near the cloud base and increases to about 55% at 30 km where ambient air temperature is lower. This large difference in N_2 fraction implies a strong initial growth by N_2 condensation. The rate of further growth is somewhat limited by the curvature (kelvin) effect until the particle size reaches micrometers. The N_2 fraction at 18 km is about 30%, similar to the laboratory value obtained by Wang et al. (2010).

Mie scattering theory is used to calculate the effective cloud optical thickness τ at wavelength 0.55 μm. For Earth's clouds to be visible to the naked eye or appear vividly on the observation images, their optical thickness τ should at least reach unity. Adopting this value as a criterion, Titan's clouds should be visible if their vertical depth is >1 km (Figure 4(f)). Under the weakest updraft, the cloud optical thickness (accumulated from the cloud base) can reach 100 and over 1000 if the convection attains a height of 23 and 30 km, respectively. With stronger updrafts, the number concentration and optical thickness become larger. The conclusion for the presence of optically thick clouds is not significantly affected by the gravitational collision–coalescence and precipitation processes ignored in the current modeling (see above).

The cloud optical thickness observed by Griffith et al. (2005, 2009) is 0.05–0.1 at mid-latitudes and is 0.1–8 at the tropics. Barth & Toon (2004) use a one-dimensional microphysical model and estimate the optical thickness of a methane cloud with a tholin core to be 0.1–10 at a size of 600–900 μm in radius. Rannou et al. (2006) report that the simulated optical thickness in the GCM model is 10–100 for polar methane clouds and 1–100 for tropical and subtropical clouds, whereas the observed mean particle radius is 10–100 μm. Our current model produces thicker clouds, but such overproduction could be greatly reduced after including gravitational collision and precipitation fall out. We also note that the optical thickness calculated in this study is an accumulated amount because of the nature of the parcel model which is zero-dimensional.

We show that cloud formation in Titan's troposphere is likely to be initiated by binary nucleation and subsequent condensation growth from both CH_4 and N_2 vapors. Earlier numerical studies tend to ignore the monomolecular homogenous nucleation mainly because it requires unrealistically high CH_4 supersaturation. Instead, tholin particles and ethane ice that formed and descended from the stratosphere are assumed to act as condensation nuclei for methane cloud formation in the troposphere. Our simulations suggest that binary nucleation also plays a role in the cloud formation process in Titan's lower atmosphere under moderate convections.

5. CONCLUSION

In this study, a multi-component microphysical model was used to understand the formation of super-cooled methane particles in the troposphere of Titan. The model originally designed for aerosol and cloud formation on Earth was modified for simulating particle formation involving CH_4 and N_2. It was first applied to simulate particle formation in a laboratory study under conditions similar to that of Titan at altitudes of 13 and 19 km. The results showed that our model can reproduce well the laboratory measurements, including the time evolution of total pressure, particle size, and number concentration, as well as the fraction of N_2 dissolved in the particles. Our results indicated that new particle formation can occur via binary nucleation of CH_4 and N_2, and the subsequent condensation growth of the particles also involves these two gases. Sensitivity tests showed that the initial plume temperature (the initial saturation ratios of CH_4 and N_2 to be more exact) is the primary factor controlling the nucleation rate, whereas the mixing–cooling time is less important. Physical–chemical parameters, including the curvature effect on surface tension and the accommodation coefficient, were tested for their contribution to model uncertainties. The former is crucial as it affects the particle number concentration by up to five orders of magnitude.

The model was then applied to simulate convective cloud formation in the troposphere of Titan. The results showed that a cloud layer could form with a base at about 19 km where the saturation ratio of CH_4 could be as much as 400% under the average conditions of Titan. The cloud base height is weakly dependent on the updraft speed, implying that air temperature and saturation ratios of CH_4 and N_2 determine the cloud formation by binary nucleation. Updraft speed (and thus the adiabatic cooling rate), on the other hand, regulates the cloud particle number concentration, which varies from 10^{-2} cm^{-3} at an updraft speed of 0.01 m s^{-1} to above 100 cm^{-3} at an updraft speed of 10 m s^{-1}. These particle concentrations are sufficient to explain the cloud layers observed on Titan. Compared with other simulations having a prescribed distribution of cloud condensation nuclei, our simulation results suggest that binary nucleation is another important mechanism for cloud formation occurring on Titan, and future modeling does need to consider this process as a source of cloud condensation

nuclei in the troposphere. Further laboratory experiments for constraining crucial physical–chemical parameters relevant to the particle formation are necessary for more sophisticated simulations. Extending our simulations to include drop freezing and subsequent solid-phase growth will also be of importance.

Special thanks is due to Chia Wang for providing the laboratory data and for helpful discussion on the experimental details. J.-P.C. and I.-C.T. acknowledge the support by NSC projects 98-2111-M-002-001 and 99-2111-M-002-009-MY3. M.C.L. is supported in part by an NSC grant 98–2111-M-001–014-MY3 to Academia Sinica.

REFERENCES

Anderson, C. M., & Samuelson, R. E. 2011, Icarus, 212, 762
Anderson, C. M., Samuelson, R. E., Bjoraker, G. L., & Achterberg, R. K. 2010, Icarus, 207, 914
Atreya, S. K., Adams, E. Y., Niemann, H. B., et al. 2006, Planet Space Sci., 54, 1177
Barth, E. L., & Rafkin, S. C. R. 2007, Geophys. Res. Lett., 34, L03203
Barth, E. L., & Toon, O. B. 2003, Icarus, 162, 94
Barth, E. L., & Toon, O. B. 2004, Geophys. Res. Lett., 31, L17S07
Barth, E. L., & Toon, O. B. 2006, Icarus, 182, 230
Bentz, J. A., Tompson, R. V., & Loyalka, S. K. 1997, Vacuum, 48, 817
Bird, M. K., Allison, M., Asmar, S. W., et al. 2005, Nature, 43, 800
Blagoi, Yu. P. 1960, Ukrayin fiz. Zh. (USSR), 5, 109
Brown, M. E., Bouchez, A. H., & Griffith, C. A. 2002, Nature, 420, 795
Chen, J.-P. 1994, J. Atmos. Sci., 51, 3505
Chen, J.-P., Hazra, A., & Levin, Z. 2008, Atmos. Chem. Phys., 8, 7431
Chen, J.-P., & Lamb, D. 1994, J. Atmos. Sci., 51, 2613
Chen, J.-P., & Lamb, D. 1999, J. Atmos. Sci., 56, 2293
Chen, J.-P., McFarquhar, G. M., Heymsfield, A. J., & Ramanathan, V. 1997, J. Geophys. Res., 102, 6637
Chen, J.-P., Tsai, T.-S., & Liu, S.-C. 2011, Atmos. Chem. Phys., 11, 7171
Doyle, G. J. 1961, J. Chem. Phys., 35, 795
Dufour, L., & Defay, R. 1963, Thermodynamics of Clouds (New York: Academic)
Firanescu, G., Hermsdorf, D., Ueberschaer, R., & Signorell, R. 2006, Phys. Chem. Chem. Phys., 8, 4149
Firanescu, G., Luckhaus, D., Patey, G. N., Atreya, S. K., & Signorell, R. 2011, Icarus, 212, 779
Fuchs, N. A. 1959, Evaporation and Droplet Growth in Gaseous Media (London: Pergamon)
Fuchs, N. A. 1964, The Mechanics of Aerosols (London: Pergamon)
Fuks, S., & Bellemans, A. 1966, Physica, 32, 594
Griffith, C. A., Hall, J. L., & Geballe, T. R. 2000, Science, 290, 509
Griffith, C. A., Owen, T., Miller, G. A., & Geballe, T. 1998, Nature, 395, 575
Griffith, C. A., Penteado, P., Baines, K., et al. 2005, Science, 310, 474
Griffith, C. A., Penteado, P., Rannou, P., et al. 2006, Science, 313, 1620
Griffith, C. A., Penteado, P., Rodriguez, S., et al. 2009, ApJ, 702, L105
Hueso, R., & Sánchez-Lavega, A. 2006, Nature, 442, 428
Kirk, B. S., & Ziegler, W. T. 1965, International Advances in Cryogenic Engineering, Vol. 10 (New York: Plenum)
Kuiper, G. P. 1944, ApJ, 100, 378
Lamb, D., & Verlinde, J. 2011, Physics and Chemistry of Clouds (Cambridge: Cambridge Univ. Press)
Le Mouélic, S., Rannou, P., Ralriguez, S., et al. 2012, Planet. Space Sci., 60, 86
Lide, D. R. 1992, CRC Handbook of Chemistry and Physics (73rd ed.; Boca Raton, FL: CRC)
Niemann, H. B., Atreya, S. K., Bauer, S. J., et al. 2005, Nature, 438, 779
Pruppacher, H. R., & Klett, J. D. 1997, Microphysics of Clouds and Precipitation (Dordrecht: Kluwer)
Rannou, P., Hourdin, F., McKay, C. P., & Luz, D. 2004, Icarus, 170, 443
Rannou, P., Montmessin, F., Hourdin, F., & Lebonnois, S. 2006, Science, 311, 201
Rodriguez, S., Le Mouélic, S., Rannou, P., et al. 2009, Nature, 459, 678
Rodriguez, S., Le Mouélic, S., Rannou, P., et al. 2011, Icarus, 216, 89
Roe, H. G., Bouchez, A. H., Trujillo, C. A., Schaller, E. L., & Brwon, M. E. 2005, ApJ, 618, L49
Roe, H. G., de Pater, I., Macintosh, B. A., & McKay, C. P. 2002, ApJ, 581, 1399
Samuelson, R. E., & Mayo, L. A. 1997, Planet. Space Sci., 45, 949
Samuelson, R. E., Smith, M. D., Achterberg, R. K., & Pearl, J. C. 2007, Icarus, 189, 63
Schaller, E. L., Brown, M. E., Roe, H. G., & Bouchez, A. H. 2006, Icarus, 182, 224
Schaller, E. L., Roe, H. G., Schneider, T., & Brown, M. E. 2009, Nature, 460, 873
Seinfeld, J. H., & Pandis, S. N. 2006, Atmospheric Chemistry and Physics: from Air Pollution to Climate Change (New York: Wiley)
Thompson, W. R., Zollweg, J. A., & Gabis, D. H. 1992, Icarus, 97, 187
Tokano, T., McKay, C. P., Neubauer, F. M., et al. 2006, Nature, 442, 432
Trafton, L. 1972, ApJ, 175, 295
Trilling, L. 1971, Surf. Sci., 27, 1
Turtle, E. P., DelGenio, A. D., Barbara, J. M., et al. 2011, Geophys. Res. Lett., 38, L03203
Turtle, E. P., Perry, J. E., McEwen, A. S., et al. 2009, Geophys. Res. Lett., 36, L02204
Upstill, C. E., & Evans, R. 1977, J. Phys. C: Solid State Phys., 10, 2791
Wagner, W. 1973, Cryogenics, 13, 470
Wang, C. C., Atreya, S. K., & Signorell, R. 2010, Icarus, 206, 787
Wanlass, F. M., & Eyring, H. 1961, Advances in Chemistry (Washington, DC: American Chemical Society)